INSTITUTE OF PHYSICS PUBLISHING NONLINEARITY

Nonlinearity **19** (2006) 1021–1047 doi:10.1088/0951-7715/19/5/002

Intermittency, metastability and coarse graining for coupled deterministic–stochastic lattice systems

M A Katsoulakis[1], **A J Majda**[2] **and A Sopasakis**[1]

[1] Department of Mathematics and Statistics, University of Massachusetts, Amherst, MA 01003, USA
[2] Courant Institute of Mathematical Sciences and Center for Atmospheric and Ocean Sciences, New York University, New York, NY 10012, USA

E-mail: markos@math.umass.edu, jonjon@cims.nyu.edu and sopas@math.umass.edu

Received 3 July 2005
Published 10 April 2006
Online at stacks.iop.org/Non/19/1021

Recommended by J P Keating

Abstract

We study the role of strong particle/particle interactions and stochastic fluctuations emanating from the micro-/sub-grid scale, in the context of a simple prototype hybrid system consisting of a scalar linear ordinary differential equation (ODE), coupled to a microscopic spin flip Ising lattice system. Due to the presence of strong interactions in the lattice model, the mean-field approximation of this system is a Fitzhugh–Nagumo-type system of ODE. However, microscopic noise and local interactions will significantly alter the deterministic and spatially homogeneous mean-field Fitzhugh–Nagumo behaviours (excitable, bistable and oscillatory) and will yield corresponding regimes with phenomena driven by the interaction of nonlinearity and noise across scales, such as strong intermittency, metastability and random oscillations. Motivated by these observations we consider a class of stochastic numerical approximations based on systematic coarse-grainings of stochastic lattice dynamics. The resulting stochastic closures give rise to computationally inexpensive reduced hybrid models that capture correctly the transient and long-time behaviour of the full system; this is demonstrated by detailed time series analysis that includes comparisons of power spectra and auto- and cross-correlations in time and space, especially in examples dominated by strong interactions between scales and fluctuations, such as nucleation, intermittent and random oscillation regimes.

Mathematics Subject Classification: 82B26, 82B27, 82B80, 82B20, 82B31, 82B22, 34C55, 34C15, 60G99

(Some figures in this article are in colour only in the electronic version)

1. Introduction

In applications ranging from catalysis and deposition processes to polymeric flows and complex biological networks and stochastic parametrizations for tropical and open ocean convection [16, 18, 20, 21, 23, 24], coupled systems of microscopic stochastic models and deterministic macroscopic ordinary and partial differential equations (ODEs/PDEs) are commonplace. In this class of problems, microscopic stochastic processes, typically simulated by Monte Carlo (MC) methods, model small scale activity, for instance adsorption, desorption, surface reaction and surface diffusion of particles on an interface or boundary layer which is in contact with a gas/fluid phase. The micro-mechanisms are thus interrelated with the large scale fluid flow modelled by continuum ODEs/PDEs describing the evolution of fluid and thermodynamic variables. Challenges in these hybrid problems arise in the direct numerical simulation of realistic size systems due to scale disparities between the discrete stochastic microscopic models and the continuum macroscopic equations; secondly, due to nonlinear interactions across a wide range of scales in the coupled system, the stochasticity inherited from the microscopic model can play a subtle but important role in the transient and long-time behaviour of the overall system.

In our earlier work [5, 6] we addressed related issues in the context of prototype mathematical models consisting of a deterministic system of ODEs coupled with a stochastic spin flip/spin exchange Ising model. In [5] we obtained deterministic mesoscopic models for this class of hybrid systems in terms of stochastic averaging, mean-field and local mean-field closures. Remarkable agreement was observed in a number of stringent, in terms of mathematical theory, parameter regimes between direct numerical simulations of hybrid systems and deterministic closures. In [6] we specifically examined the influence of sub-grid scale noise in such hybrid systems when phase transitions do not occur in the microscopic lattice dynamics, but the rather complex dynamic behaviour is primarily due to the bifurcations of the externally coupled deterministic system, and its coupling with the microscopic stochastic model. Long-time simulations and asymptotic analysis strongly suggested that, in general, deterministic closures of a hybrid system such as the ones considered in [5] may be either inadequate as descriptions of the overall system or simply difficult to both derive and assess for effectiveness. For example, fluctuation-driven rare events occur in several parameter regimes and are not captured by the deterministic mesoscopic equations; this fact can be mathematically quantified in the case of stochastic averaging for systems of stochastic differential equations, using large deviation methods [3]. Similar issues may also arise when strong noise is present in the system, in which case fluctuations play a dominant role in the overall dynamics, for instance noise is important when the external deterministic system exhibits multiple steady states (e.g. bistability) or when bifurcations of various types arise [6]. As in the case of their analytic counterparts, computational closure methods relying on relatively short runs of micro-simulators such as the equation-free [12] and HMM [2] approaches may also have to account for such fluctuation-driven phenomena when determining the integration time for the micro-simulation or the proper coarse-grained observables such as a number of moments.

In this paper we continue our earlier work on hybrid systems and study the intrinsically more complex case where randomness, macroscopic dynamics, and microscopic interactions in the stochastic lattice system compete and possibly dramatically affect the overall hybrid system behaviour. More specifically, in the presence of strong particle/particle interactions in the lattice system compared to the random fluctuations, the mean-field approximation of the proposed hybrid system gives an initial insight into the overall dynamics: the mean-field system is a spatially homogeneous Fitzhugh–Nagumo-type system of ODEs that exhibits in different parameter regimes, excitable, oscillatory and bistable behaviours. Therefore, it is not

surprising that the presence of noise will substantially modify these deterministic behaviours and yield corresponding regimes with phenomena driven by the interaction of nonlinearity and noise across scales, such as strong intermittency, metastability, and random oscillations. A particularly simple example of these subtle behaviours is demonstrated in section 5, where we consider a hybrid system with uniform, Curie–Weiss type interactions in the microscopic lattice dynamics; we recall here that the uncoupled Curie–Weiss spin model is an important example in statistical physics that exhibits phase transitions, hysterisis, critical fluctuations and other related phenomena and allows fairly simple yet revealing analytical calculations [1, 17].

Motivated by the aforementioned critical interplay between interactions across scales and random fluctuations, we consider a class of stochastic closures that yield a computationally more efficient hybrid system but still capture correctly the transient and long-time behaviour of the full hybrid system. Such stochastic closures were first developed in [6] for hybrid systems without phase transitions in the microscopic dynamics, as well as in [14] as a stochastic parametrization of unresolved features of tropical convection, and are based on systematic coarse-grainings of (uncoupled) stochastic lattice dynamics that were developed in [7, 8, 11]. In section 6 we demonstrate in terms of detailed comparisons to direct numerical simulations, that the coarse-grained stochastic closures yield statistical agreement with the full hybrid system; in particular we carry out time series analyses that include comparisons of power spectra and, auto- and cross-correlations in time and space in the aforementioned intermittent, metastable and random oscillation regimes.

2. Hybrid model

We first introduce the microscopic spin flip stochastic Ising process $\{\sigma_t\}_{t\geqslant 0}$, modelling the adsorption and desorption of particles on a one-dimensional surface, coupled to an ODE that serves as a caricature of an overlying gas-phase dynamics. The stochastic process is completely determined by its generator L and the two-way coupled system is written as

$$\frac{\mathrm{d}}{\mathrm{d}t}X = \frac{1}{\tau_c}(a\bar{\sigma} + b - cX), \tag{1}$$

$$\frac{\mathrm{d}}{\mathrm{d}t}Ef(\sigma) = EL_X f(\sigma) \tag{2}$$

where $\bar{\sigma}$ denotes a spatial average coverage, f is a test function, τ_c corresponds to the characteristic time for the ODE model and a, b and c are parameters which are provided explicitly for each example considered in the simulations in section 6. We denote by L_X the generator of the microscopic model, where the subscript X denotes the dependence of (2) on (1). Here we focus on the case of strong interaction/low temperature where phase transitions occur in the stochastic system. Examples of hybrid systems such as (1), (2) and scalar equations with bistable behaviour or saddle node bifurcations, as well as spatially homogeneous complex Ginsburg–Landau equations exhibiting Hopf bifurcations have been studied in [6] in regimes without phase transitions in the lattice system. In contrast to these earlier studies, if $\bar{\sigma}$ is constant in (1), the resulting ODE is linear with trivial behaviour, without any external bifurcations; thus here the focus is on the role of complex dynamics with phase changes in the microscopic lattice dynamics on the overall coupled system (1), (2).

We next provide a detailed description of the system (1), (2). We consider a microscopic stochastic model defined on a periodic lattice of size N which we denote by $\mathcal{L} = (1/N)Z \cap [0, 1]$. At each lattice site $x \in \mathcal{L}$, the order parameter, $\sigma(x)$, is allowed to take the value 0 or 1. In accordance with the classical Ising model we refer to the order parameter as spin. We will assume that sites cannot be occupied by more than one particle (exclusion principle).

A spin configuration σ is an element of the configuration space $\mathcal{H}_{N,1} = \{0, 1\}^{\mathcal{L}}$ and we write $\sigma = \{\sigma(x) : x \in \mathcal{L}\}$, denoting by $\sigma(x)$ the spin at x. Physically this mechanism may describe the desorption of a particle from a surface described by the lattice to the gas phase above and conversely the adsorption of a particle from the gas phase to the surface. Similarly it can describe phase transitions without order parameter conservation.

The stochastic process $\{\sigma_t\}_{t\geqslant 0}$ is a continuous time jump Markov process on $L^\infty(\mathcal{H}_{N,1}, R)$ with generator [15]

$$L_X f(\sigma) = \sum_{x\in\mathcal{L}} c(x,\sigma)[f(\sigma^x) - f(\sigma)] \tag{3}$$

for any test function $f \in L^\infty(\mathcal{H}_{N,1}, R)$. Here $c(x,\sigma)$ denotes the rate of a spin flip at x for the configuration σ (see 6) and σ^x signifies the configuration after a flip at x,

$$\sigma^x(y) = \begin{cases} 1-\sigma(x), & \text{if } y = x, \\ \sigma(y), & \text{if } y \neq x. \end{cases}$$

Since there are $N = |\mathcal{L}|$ sites on the lattice, the system can be in any of $2^{|\mathcal{L}|}$ possible states while the energy of any particular state is given by the following Hamiltonian,

$$H(\sigma) = -\frac{1}{2}\sum_{x\in\mathcal{L}}\sum_{y\neq x} J(x,y)\sigma(x)\sigma(y) + \sum_x h\sigma(x), \tag{4}$$

where $J(x, y)$ is an inter-particle potential and h is a given external potential. We let

$$J(x,y) = \frac{1}{2L+1} V\left(\frac{|x-y|}{2L+1}\right),$$

where L denotes the range of microscopic interactions. Here V is assumed to be even, $V(r) = V(-r)$ and as an example we can take [7]

$$V(r) = \begin{cases} J_0 & \text{if } 0 \leqslant r \leqslant 1 \\ 0 & \text{otherwise,} \end{cases}$$

where J_0 is a parameter which based on its sign describes attractive, repulsive or non-interactions. For attractive microscopic interactions for instance, J_0 is positive.

By applying a spin flip stochastic model we create new states from old ones generated by a Markov process as described below. Equilibrium states of the stochastic model are described by the canonical Gibbs states at the prescribed temperature T. If we denote the inverse temperature by $\beta = 1/(kT)$ we then have

$$\mu_{\beta,N}(\mathrm{d}\sigma) = \frac{1}{Z}\mathrm{e}^{-\beta H(\sigma)} P_N(\mathrm{d}\sigma), \tag{5}$$

where $P_N(\mathrm{d}\sigma)$ denotes the (product) prior distribution on $\mathcal{L}$,

$$P_N(\mathrm{d}\sigma) = \prod_{x\in\mathcal{L}} \rho(\mathrm{d}\sigma(x)) \qquad \text{and} \qquad \rho(\sigma(x)=0) = \frac{1}{2}, \quad \rho(\sigma(x)=1) = \frac{1}{2}.$$

Here Z is the partition function, guaranteeing that (5) is a probability measure.

In this model we implement spin flip Arrhenius dynamics. Under this type of mechanism the simulation is driven based on the energy barrier a particle has to overcome in flipping from one state to another given by (7) below. For Metropolis and other choices of dynamics see [7]. The Arrhenius spin flip rate $c(x,\sigma)$ at lattice site x and spin configuration σ is given by

$$c(x,\sigma) = \begin{cases} c_d \mathrm{e}^{-\beta[U_0+U(x)]}, & \text{when } \sigma(x) = 0, \\ c_a & \text{when } \sigma(x) = 1, \end{cases} \tag{6}$$

where

$$U(x) = \sum_{\substack{z \neq x \\ z \in \mathcal{L}}} J(x, z)\sigma(z) - h \tag{7}$$

with adsorption/desorption constants

$$c_a = c_d = 1/\tau_I$$

and τ_I denoting the characteristic time of the stochastic process. Here U_0 represents the energy associated with the surface binding of the particle at location x which we absorb in h setting $U_0 = 0$. In general we write the spin flip rate (6) as

$$c(x, \sigma) := c_a(x, \sigma) + c_d(x, \sigma) = c_a(1 - \sigma(x)) + c_d\sigma(x)\exp(-\beta(U_0 + U(x)), \tag{8}$$

and the probability of a spin flip at x during time $[t, t+\Delta t]$ is $c(x, \sigma)\Delta t + O(\Delta t^2)$. The dynamics as described here leave the Gibbs measure (5) invariant, since they satisfy the detailed balance condition [7].

Overall the ODE (1) is coupled to the stochastic model through the area fraction (or total coverage) defined as the spatial average of the stochastic process σ,

$$\overline{\sigma} = \frac{1}{N}\sum_{x \in \mathcal{L}} \sigma(x). \tag{9}$$

On the other hand, the stochastic model (2) is coupled to the ODE through the application of an external potential

$$h \equiv h(X) = \alpha X + \gamma \tag{10}$$

for constants α and γ whose values are specified for each case examined.

3. Deterministic closures and the role of stochastic fluctuations

In this section we outline some deterministic closures of the hybrid system (1), (2) studied in [6] in the distinct asymptotic limit of weak long range interactions $L \to \infty$. In this case we obtain a coupled, possibly spatially distributed mean-field deterministic mesoscopic system for the evolution of X and the average local coverage corresponding to the stochastic order parameter σ without any time-scale separation assumption. In this case equilibrium mean-field theory becomes asymptotically exact (see [5] for the rigorous derivations for these and other closures).

We briefly outline here the derivation of mean-field equations for our coupled system (1), (2). We consider the spin flip Arrhenius type dynamics which was presented in section 2, and obtain a time evolution law for the empirical measure,

$$\mu^N(\mathrm{d}y, t) = \frac{1}{N}\sum_{x \in \mathcal{L}} \sigma_t(x)\delta_x(\mathrm{d}y), \qquad \text{for } y \in R. \tag{11}$$

Note that if $A \subset R$ then

$$\mu^N(A, t) = \frac{\text{number of particles in } A}{N}. \tag{12}$$

Passing to the weak-$*$ limit in $\mu^N(\mathrm{d}y, t)$ and for a smooth long-ranged potential $J(x, y) = (1/N)V(|x - y|/N)$ and any finite time T, we have

$$\lim_{N\to\infty} X(t) = Y(t) \quad \text{and} \quad \lim_{N\to\infty} \mu^N(\mathrm{d}y, t) = u(y, t)\,\mathrm{d}y \qquad \text{uniformly in } [0, T], \tag{13}$$

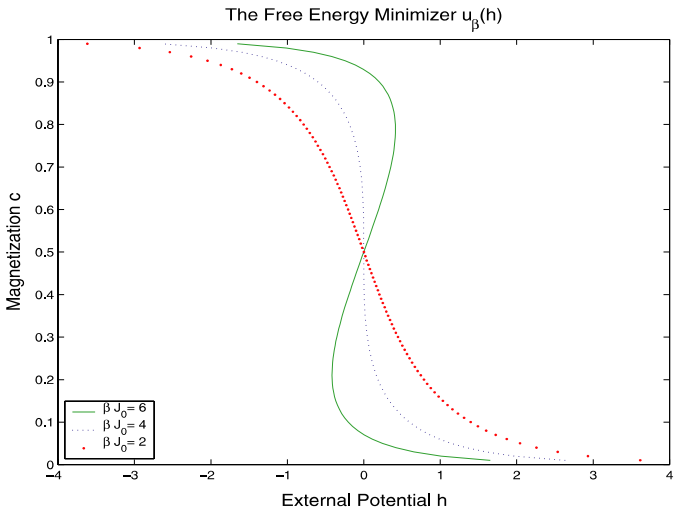

Figure 1. The total coverage for the uncoupled $\bar{u}$ from [5] for different values of $\beta J_0 = 2, 4$ and 6 versus fixed, not depending on X, $h \equiv h(X)$ external potential. The critical point for the $\{0, 1\}$ spins satisfies $\beta_c J_0 = 4$. The hysteresis shape of the curve for the phase transition regime, $\beta J_0 = 6$, manifests the existence of two equilibria in the neighbourhood of the zero external field.

where (X, σ) are the solutions of (1), (2) and (Y, u) solves

$$\begin{cases} \dfrac{\mathrm{d}}{\mathrm{d}t} Y = \dfrac{1}{\tau_c}(a\bar{u} + b - cY), \\ \dfrac{\mathrm{d}}{\mathrm{d}t} u = \dfrac{1}{\tau_I}(1 - u - u\mathrm{e}^{-\beta V * u + \beta h(Y)}) \end{cases} \qquad \text{for } t \in [0, T] \tag{14}$$

and

$$\lim_{N\to\infty} \bar{\sigma}(t) = \lim_{N\to\infty} \int_0^1 \mu^N(dy, t) = \int_0^1 u(x, t)\, dx = \bar{u}(t).$$

Relation (13) is analogous to the law of large numbers yielding the mean behaviour of the hybrid system and treating fluctuations as a higher order correction.

A simple but important special case follows if we consider the Curie–Weiss analogue of the hybrid system (1, 2), i.e. by considering a constant potential $V(x - y) \equiv J_0$ uniformly for all x, y on the microscopic lattice. It is a simple consequence of (14) to obtain in the $N \to \infty$ limit the following mean-field model ODE system,

$$\text{mean-field model} \begin{cases} \dfrac{\mathrm{d}}{\mathrm{d}t} Y = \dfrac{1}{\tau_c}(a\bar{u} + b - cY), & (15a) \\ \dfrac{\mathrm{d}\bar{u}}{\mathrm{d}t} = \dfrac{1}{\tau_I}(1 - \bar{u}) - \dfrac{1}{\tau_I}\bar{u}\mathrm{e}^{-\beta J_0 \bar{u} + \beta h(Y)} & (15b) \end{cases} \qquad \text{for } t \in [0, T].$$

We note here that the (uncoupled) Curie–Weiss lattice spin model of (2) is a classical simple example in statistical mechanics that exhibits phase transitions even in one space dimension and allows detailed explicit calculations such as mean-field and thermodynamic limits at all temperatures. For example, the phase transition regime for the microscopic lattice system which appears for $\beta J_0 > 4$ can be seen in figure 1. As further detailed in section 5, the Curie–Weiss hybrid system analogue can provide some first insights in a simple context on the influence of noise and phase transitions on the overall hybrid system dynamics by comparing it

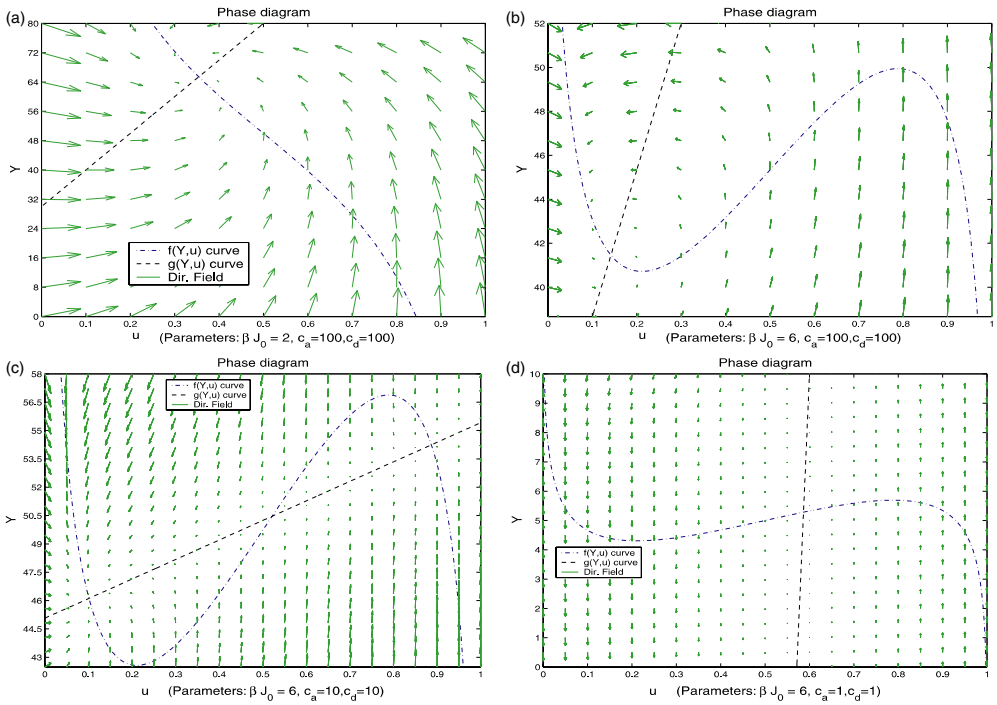

Figure 2. Direction field for mean-field system (15) under different parameter regimes. Here $f(Y, u)$ and $g(Y, u)$ correspond to the top and bottom equations of (15), respectively. Cases of excitability for $\beta J_0 = 2$ and excitability, bistability and oscillations for $\beta J_0 = 6$, respectively. Compare with pp 328–9 of [19].

against the mean-field closure (15). In fact, this example underlines some of the shortcomings of deterministic closures and motivates the stochastic closures in the following section that can allow us to overcome the related issues.

We next examine in more detail the behaviour of the mean-field closure (15) with respect to different values of βJ_0. The phase portrait of the mean-field system (15) for $\beta J_0 = 2$ and $\beta J_0 = 6$ is shown in figure 2. Note that in the regime $\beta J_0 < \beta_c J_0 = 4$, shown in figure 2, the zero level curve of the bottom equation in (15) is monotone and can only produce a single stable state. This is in sharp contrast to the much richer behaviour which the mean-field system (15) displays when $\beta J_0 > 4$ (see the remaining three subplots of figure 2). Indeed, we observe excitable (figure 2(b)), bistable (figure 2(c)) and oscillatory (figure 2(d)) stability profiles, depending on the parameters chosen for the mean-field system (15) in the regime $\beta J_0 = 6$ depicted in figure 2. As mentioned above, in the uncoupled lattice system, when $\beta J_0 > 4$, the mean-field equation in (15b) exhibits phase transitions in the sense that bistability occurs, as also seen in the non-monotone zero level curves of (15b) in figure 2 or the multivalued curve in figure 1. In the case of the fully coupled system (15), the phase transition regime $\beta J_0 > 4$ in the isolated lattice system marks the onset of three nontrivial regimes, excitability, bistability and oscillations. The bistability regime is associated with phase transitions in the overall hybrid system, while excitability and oscillations are substantially different from the trivially stable regime seen when $\beta J_0 < 4$ (see figure 2(a)).

A catalysis system which is essentially equivalent to (15), at least in the ODE case, was first studied in [13], predicting oscillations both in the coverage and the pressure but in the absence

of fluctuations, detailed interactions and spatial inhomogeneities. For this system, comparisons between mean-field and Monte Carlo simulations [23] showed that in many parameter regimes there is substantial agreement attributed to the coupling with the well-mixed gas-phase; drastic discrepancies were also observed, as well as a variety of dynamic and equilibrium behaviours, depending on the separation of time scales between individual micro-mechanisms and the time scale of the ODE. Furthermore we note that system (15) has the same behaviour as a typical Fitzhugh–Nagumo ODE system,

$$\frac{\mathrm{d}}{\mathrm{d}t}x = au + b - cx, \qquad \text{and} \qquad \frac{\mathrm{d}}{\mathrm{d}t}u = g(u) - x, \tag{16}$$

where $g(u) = u(\omega - u)(u - 1)$ [19] (p 329). In fact, system (16), displays a phase portrait similar to (15) for $\beta J_0 > 4$.

The mean-field closure (15) provides some first insights on the overall dynamics of the full hybrid system (1), (2) by suggesting the presence of excitable, bistable and oscillatory regimes. However the noise in the hybrid system is expected to substantially modify these deterministic regimes, potentially yielding corresponding behaviours of strong intermittency, metastability and random oscillations. Therefore incorporating stochasticity in any closure scheme is essential for both modelling and simulation purposes. In this latter direction we propose in the following section a stochastic closure which, as we will show with extensive numerical simulations in sections 5 and 6, can address such issues by accurately approximating the microscopic hybrid solutions through coarse graining.

4. Coarse-graining and stochastic closures

Motivated by the examples in section 3 where stochastic noise is expected to play a crucial role in transient and long-time dynamics, we pursue the derivation of stochastic approximations of the hybrid models that will allow both enhanced computational efficiency and improved accuracy in closure approximations. More precisely, we obtain stochastic closures of the hybrid system in terms of a coupled ODE with a coarse-grained stochastic lattice model. Stochastic coarse-grained closures for uncoupled lattice systems were first introduced in [7,8,11]. Here we extend these methods to hybrid systems in the presence of phase transitions in the microscopic lattice dynamics. Our key goal in this section will be to formulate a reduced description which contains more detail in terms of interactions and stochastic fluctuations than mean-field equations.

4.1. Coarse graining of the hybrid system

Keeping in mind quantity (12) defined in terms of the empirical measure μ_N we define the coarse-grained random process

$$\eta(k) = \mathcal{T}(\sigma)(k) := \sum_{x \in D_k} \sigma(x), \qquad \text{for } k = 1, \ldots, n.$$

for $k \in \{0, 1, \ldots, m\}$, where the coarse lattice $\mathcal{L}_c$ is defined as $\mathcal{L}_c = (1/m)Z \cap [0, 1]$ where $\mathcal{L}_c \subset \mathcal{L} = (1/N)Z \cap [0, 1]$ and $\eta(k) \in \{0, 1, \ldots, q\}$ the coverage of the coarse cell $D_k = (1/N)Z \cap [k/m, (k + 1)/m]$ for $1 \leqslant k \leqslant m$ and $N = mq$. Note that each D_k consists of q microcells and the order parameter $\eta(k)$ counts the number of particles in each coarse cell D_k. We define the coarse configuration space $\mathcal{H}_{m,q} = \{0, 1, \ldots, q\}^{\mathcal{L}_c}$. For any test function $g \in L^\infty(\mathcal{H}_{m,q}; R)$ we can define

$$f(\sigma) := g(\mathcal{T}(\sigma)) = g(\eta),$$

where f is a test function in $L^\infty(\mathcal{H}_{N,1}; R)$. Therefore (2) with generator (3) can be written as follows in terms of the coarse lattice $\mathcal{L}_c$,

$$\frac{\mathrm{d}}{\mathrm{d}t}Ef(\sigma) = E\sum_{x\in\mathcal{L}} c(x,\sigma)[f(\sigma^x) - f(\sigma)] = E\sum_{k\in\mathcal{L}_c}\sum_{x\in D_k} c(x,\sigma)[f(\sigma^x) - f(\sigma)]. \tag{17}$$

For $x \in D_k$ we have

$$\mathcal{T}(\sigma^x)(k) = \sum_{y\in D_k}\sigma^x(y) = \begin{cases}\eta(k)+1 & \text{when } \sigma(x) = 0,\\ \eta(k)-1 & \text{when } \sigma(x) = 1.\end{cases}$$

Thus the right-hand side of (17) can be expressed in terms of g as

$$f(\sigma^x) - f(\sigma) = (1-\sigma(x))[g(\eta+\delta_k) - g(\eta)] + \sigma(x)[g(\eta-\delta_k) - g(\eta)],$$

where $\delta_k \in \mathcal{H}_{m,q}$ denotes the configuration with a single particle at site $k \in \mathcal{L}_c$. Rearranging the summations accordingly in (17) we obtain

$$\frac{\mathrm{d}}{\mathrm{d}t}Eg(\eta) = \frac{\mathrm{d}}{\mathrm{d}t}Ef(\sigma) = E\sum_{k\in\mathcal{L}_c} c_a(k)[g(\eta+\delta_k) - g(\eta)] + c_d(k)[g(\eta-\delta_k) - g(\eta)], \tag{18}$$

where $g \in L^\infty(\mathcal{H}_{m,q}; R)$ is a test function and $c_a(k)$, $c_d(k)$ denote the exactly coarse-grained adsorption and desorption rates,

$$c_a(k) = \sum_{x\in D_k} c(x,\sigma)(1-\sigma(x)), \qquad c_d(k) = \sum_{x\in D_k} c(x,\sigma)\sigma(x).$$

Note that up to this point these rates depend on the microscopic configuration σ and not on the coarse random variable $\mathcal{T}(\sigma)$. In order to derive a Markov process for the coarse variable η we need to express these rates in terms of η. Indeed for the adsorption we readily have

$$c_a(k) = \sum_{x\in D_k} c(x,\sigma)(1-\sigma(x)) = \sum_{x\in D_k} d_0(1-\sigma(x)) = d_0[q-\eta(k)], \tag{19}$$

where $d_0 = 1/\tau_I$ and $U_0 = 0$ as before. Based on relation (19) we can therefore define the coarse-grained adsorption rate

$$c_a^{cg}(k,\eta) = d_0[q-\eta(k)], \tag{20}$$

which denotes the rate by which $\eta(k)$ is increased by 1. We wish to obtain a similar relation for the desorption,

$$\begin{aligned} c_d(k) &= \sum_{x\in D_k} c(x,\sigma)\sigma(x) = d_0\sum_{x\in D_k}\sigma(x)\mathrm{e}^{-\beta(U_0+U(x))}\\ &= d_0\sum_{x\in D_k}\sigma(x)\mathrm{e}^{-\beta(U_0+U(x))} = \mathrm{e}^{-\beta(U_0+\bar{U}(k)+O(q/(2L+1)))}\sum_{x\in D_k} c_0\sigma(x)\\ &= d_0\eta(k)\mathrm{e}^{-\beta(U_0+\bar{U}(k))}\exp\left[O\left(\frac{q}{2L+1}\right)\right], \end{aligned} \tag{21}$$

where we used the approximation $U(x) = \bar{U}(k) + O(q/(2L+1))$, where [7]

$$\bar{U}(k) = \sum_{\substack{l\in\mathcal{L}_c\\ l\neq k}}\bar{J}(k,l)\eta(l) + \bar{J}(0,0)(\eta(k)-1) - h(X) \tag{22}$$

and the coarse-grained interaction potential $\bar{J}(k,l)$ is computed as the average of pair-wise interactions between microscopic spins on coarse cells D_k and D_l,

$$\bar{J}(l,k) = q^2\int_{D_k}\int_{D_l} J(r-s)\,\mathrm{d}r\,\mathrm{d}s.$$

When $q \ll L$ we may disregard the $\exp[O(q/(2L+1))]$ term in (21), treating it as an error, and obtain the approximate desorption coarse-grained rate,

$$c_d^{cg}(k,\eta) = d_0\eta(k)\mathrm{e}^{-\beta(U_0+\bar{U}(k))}. \tag{23}$$

Based on rates (23) and (20) we can now provide the coarse-grained Markov process generator for η based on (18),

$$L_c g(\eta) = \sum_{k\in\mathcal{L}_c} c_a^{cg}(k,\eta)[g(\eta+\delta_k)-g(\eta)] + c_d^{cg}(k,\eta)[g(\eta-\delta_k)-g(\eta)], \tag{24}$$

and the corresponding coarse-grained dynamics,

$$\frac{\mathrm{d}}{\mathrm{d}t}Eg(\eta) = EL_c g(\eta), \qquad \text{where } g \in L^\infty(\mathcal{H}_{m,q}; R).$$

Since $\bar{\eta} = \bar{\sigma}$, the coarse-grained hybrid system (1), (2) becomes

$$\begin{aligned} \frac{\mathrm{d}}{\mathrm{d}t}X &= \frac{1}{\tau_c}(a\bar{\eta}+b-cX), \\ \frac{\mathrm{d}}{\mathrm{d}t}Eg(\eta) &= EL_c g(\eta). \end{aligned} \tag{25}$$

System (25) yields a stochastic closure of the original system since no linearization arguments or use of expected values are involved. Note that in fact for this approximation to work we only require that $2L+1 \gg q$ and not necessarily that $N \to \infty$ as is the case for the deterministic closures. We will present further numerical as well as theoretical results showing the capabilities and possible limitations of this stochastic coarse-grained closure in the following section and in section 6.

4.2. Uncoupled coarse-grained stochastic dynamics

We begin with a theoretical estimate for the uncoupled dynamics case that gives a first concrete indication regarding the regimes of validity of the method. First we define the concept of relative entropy that will provide a measure of accuracy for the proposed coarse-grained procedure. We consider two probability measures $\pi_1(\sigma)$ and $\pi_2(\sigma)$ on the discrete state space $\mathcal{H}_{N,1} = \{0,1\}^{\mathcal{L}}$. We similarly denote $\mathcal{H}_{m,q} = \{0,1,\ldots,q\}^{\mathcal{L}_c}$ as the coarse-grained analogue of $\mathcal{H}_{N,1}$. We further define the relative entropy for these measures as

$$\mathcal{R}(\pi_1|\pi_2) = \sum_{\sigma\in\mathcal{S}} \pi_1(\sigma)\log\frac{\pi_1(\sigma)}{\pi_2(\sigma)}.$$

There is an important inequality which allows us to view the relative entropy as a tool for estimating distance between two measures [22],

$$\mathcal{R}(\pi_1|\pi_2) \geqslant \frac{1}{2}\left(\sum_{\sigma\in\mathcal{S}}|\pi_1(\sigma)-\pi_2(\sigma)|\right)^2 \equiv \frac{1}{2}\|\pi_1-\pi_2\|_1^2.$$

In order to compare the process $\{\mathcal{T}\sigma\}_{t\geqslant 0}$ and $\{\eta\}_{t\geqslant 0}$ we need to carry out an a priori analysis on the space of all right-continuous paths $\eta_t : [0,\infty] \to \mathcal{H}_{m,q}$ which we denote by $\mathcal{D}(\mathcal{H}_{m,q})$. We also denote by $Q_{\sigma_0,[0,T]}$ the measure on $\mathcal{D}(\mathcal{H}_{N,1})$ for the process on the interval $[0,T]$, $\{\sigma_t\}_{t\in[0,T]}$ with the initial distribution σ_0. Similarly $Q^c_{\eta_0,[0,T]}$ denotes the measure on the coarse path space $\mathcal{D}(\mathcal{H}_{m,q})$. With a slight abuse of notation we also use $\mathcal{T}_*Q$ to denote the projection of the measure Q on the coarse path space, i.e., the exact coarsening of the measure Q. Based on these definitions we have the following theorem.

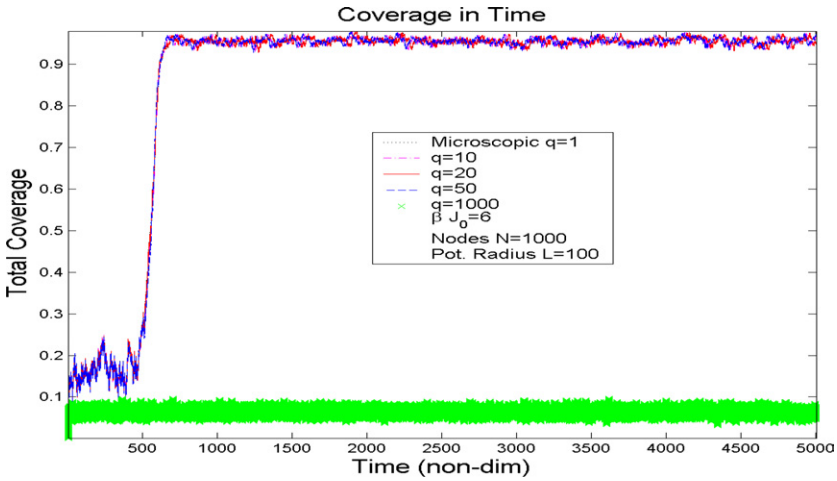

Figure 3. Microscopic versus several different coarse-grained dynamics for the uncoupled stochastic model (2) in the phase transition regime $\beta J_0 = 6 > \beta_c J_0 = 4$. The coarse-grained dynamics seem to both follow the microscopic dynamics to the correct equilibrium dynamics and capture correctly the noise on its transition path towards equilibrium. Further, all coarse grainings undergo a phase transition at the exact same time instant. As expected the birth–death case of $q = 1000$ does not attain the phase transition (see section 5 for more details on the birth–death process). Other parameters: $L = 100$, $N = 1000$.

Theorem 4.1. *Suppose the process* $\{\eta_t\}_{t\in[0,T]}$ *defined by the coarse generator* L_c *is the coarse approximation of the microscopic process* $\{\sigma_t\}_{t\in[0,T]}$. *Then for any* $q < L$ *and* N *where* $mq = N$ *the information loss as* $q/L \to 0$ *is*

$$\frac{1}{N}\mathcal{R}(\mathcal{T}_* Q_{\mathcal{T}_*\sigma_0,[0,T]} | Q^c_{\eta_0,[0,T]}) = T\,O\left(\frac{q}{2L+1}\right). \tag{26}$$

We refer to [10] for the proof. The relative entropy estimate above demonstrates the limitations of the coarse-graining method since it gives an order 1 error for nearest neighbour interactions ($L = 1$). This is not surprising in view of well-known renormalization calculations for the Ising model, as well as explicit numerical comparisons [7]. On the other hand, (21) identifies a small parameter in the coarse-graining process, namely the ratio $q/(2L + 1)$. Although the estimate in theorem 4.1 is for finite times $[0, T]$ only, and grows with T, it is still useful; in the case of phase transitions in the microscopic lattice the estimate ensures numerical accuracy during nucleation, which is typically an initial stage of the evolution, see figure 4. We refer to simulations partly motivated by our rigorous results in [9] that make precisely this point. In addition we have the fact that the coarse-grained Gibbs measure, which we denote by $\mu^{cg}_{m,q}$, lies within a controlled error from the exact coarse-grained measure [11]. More specifically, we easily obtain the equilibrium version of theorem 4.1, namely

$$\frac{1}{N}\mathcal{R}((\mathcal{T}_*\mu^N)|\mu^{cg}_{m,q}) = O\left(\frac{q}{2L+1}\right). \tag{27}$$

Overall theorem 4.1 and the Gibbs measure estimate (27) imply that the transient and the long time dynamics are expected to be captured accurately by the coarse-grained closure. This is also observed in the simulations below in figures 3 and 4.

The simulations in figure 3 provide a visual indication that the coarse graining closure displays remarkable agreement with respect to the microscopic process. The coarse-grained closure presented in this figure tracks well not only the path to equilibrium but also the respective

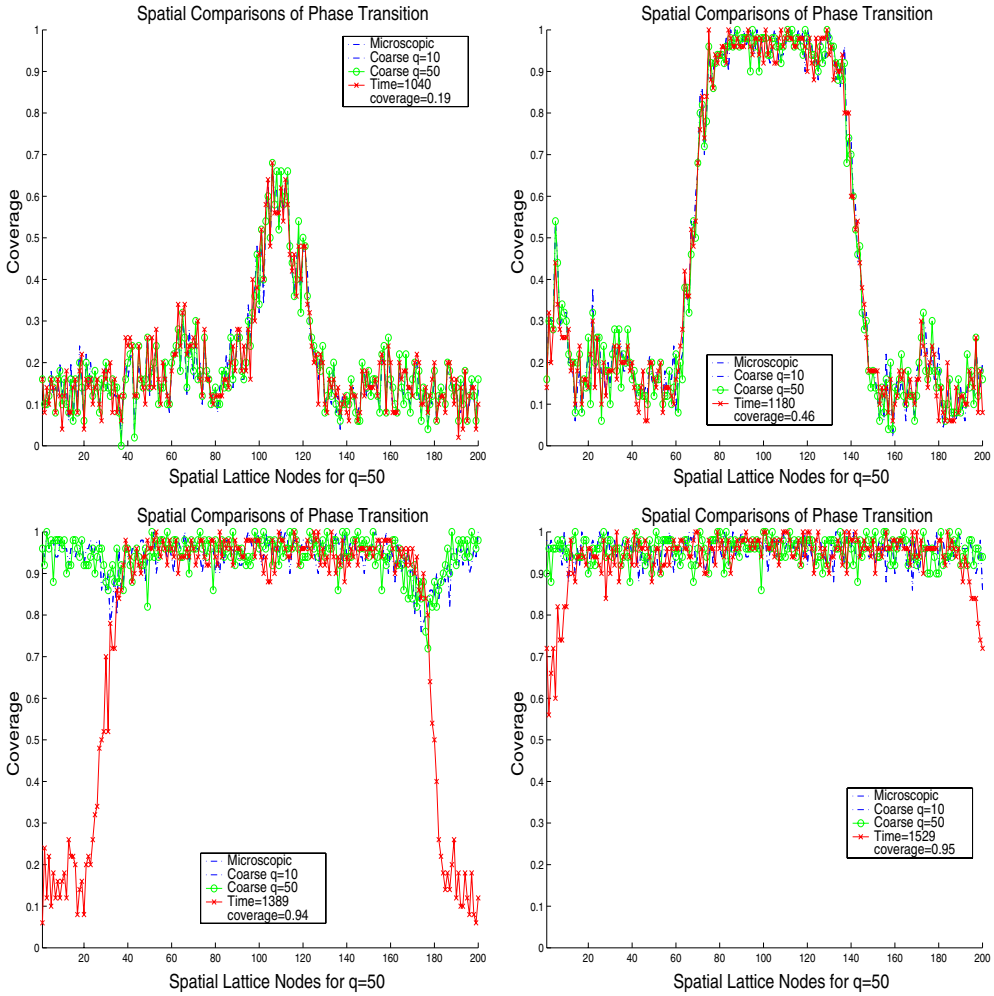

Figure 4. Snapshots of the phase transition starting from zero initial spatial distribution. Comparisons between the microscopic $q = 1$ and two coarse-grained simulations $q = 10$ and $q = 50$. The interaction radius is set to $L = 200$ while the total nodes are $N = 10\,000$. The snapshots in this simulation correspond to figure 3 with the exception that here we increased the lattice size and potential.

noise in time. However this is not entirely surprising due to theorem 4.1 and (27) as well as the large deviation principle demonstrated in [7] when $N = 2L + 1$. The simulations presented above and those which follow for hybrid systems are partly justified by the estimate in theorem 4.1.

One quantity of interest that can be calculated from the simulations is the mean time to reach, for the first time, a phase transition. This quantity is calculated as the expected value of the random exit time $\tau_1 = \inf\{t > 0 : \bar{\sigma}_t \geqslant C^+\}$, where $\bar{\sigma}_t$ denotes the total coverage at time t and $C^+ = 0.9$ (see figure 3). We then obtain $\bar{\tau}_1 = E\tau_1$ over 5000 realizations for each level of coarse graining and calculate the relative error with respect to the microscopic dynamics. The results of this calculation as well as the particular CPU times corresponding to figure 3 for each dynamics used are shown in table 1. We further note that the results in table 1 also attest to

Table 1. CPU time and relative error for uncoupled dynamics to reach phase transition. The error is the relative difference between the coarse-grained and the exact mean time $\bar{\tau}_1$. Simulation and parameters correspond to figure 3.

q	1	2	4	5	10	20	25	50	100
Rel. error %	0	0.01	0.22	0.38	0.82	3.42	4.91	17.69	77.73
CPU (s)	309 647	132 143	86 449	58 412	38 344	16 215	7 574	4 577	345

the accuracy of the coarse-grained dynamics in relation to CPU time speed-up. Table 1 shows that we incur a less then 5% relative error for the coarse-grained approximation of the phase transition time τ_1 corresponding to $q = 25$ while, at the same time, we gained a speed-up of approximately 40 times.

The last set of simulations deals with the pathwise behaviour on the spatial configuration space for nucleation of a new phase. This is an equivalent simulation to that presented in figure 3 but with N increased to 10 000 nodes for a higher resolution. We present only a qualitative comparison in the series of snapshots in figure 4 of the phase transition from the uniform (zero) initial coverage to the full coverage. We observe pathwise agreement on the configuration space even for relatively low values of q compared to the interaction radius L (e.g. $q/L \sim 1/20$). However, as the ratio q/L increases the corresponding coarse-grained process lags behind (e.g. $q/L \sim 1/4$). On the other hand, as table 1 suggests, coarser observables such as the switching times in figure 3 are well approximated by a coarser process (e.g. relative errors around 5% for $q/L \sim 1/4$), while a finer resolution is necessary for resolving detailed questions such as nucleation of new phases through islands.

In conclusion, we remark that the performance during metastability for the uncoupled spin flip system demonstrates the effectiveness of the method both in accuracy as well as in CPU gains in a very demanding set-up. We refer to [9] for further detailed computational comparisons in metastable regimes for (uncoupled) stochastic lattice systems, as well as related rigorous time-dependent numerical estimates in the weak topology.

5. The Curie–Weiss hybrid system

The uncoupled Curie–Weiss spin model with a uniform interaction potential $V(x - y) \equiv J_0$ for all x, y on the microscopic lattice is a classic simple example in statistical mechanics that exhibits phase transitions even in one space dimension (see figure 1) and allows detailed explicit calculations such as mean-field and thermodynamic limits at all temperatures [1, 17]. Here we introduce an analogue of the Curie–Weiss spin system for the hybrid systems (1, 2). As discussed in section 3 such a system gives rise to the mean-field ODE (15) in the $N \to \infty$ limit. We will first examine in this simplest context the influence of noise and phase transitions on the overall hybrid system dynamics by comparing it against the mean-field closure (15) presented in section 3. The examples which we present in this section underline some of the limitations of deterministic closures and at the same time motivate the numerical simulations of the stochastic closure in section 6 which decidedly resolve the aforementioned shortcomings.

Based on the assumption of uniform particle/particle interactions and the coarse-grained closure presented in section 4 we derive here an exact birth–death type stochastic closure for the Curie–Weiss hybrid system in the sense that there is no error in the approximation: we revisit the coarse-grained closure derived in section 4.1 and especially the error term in the desorption rate $c_d(k)$ which is responsible for this closure being an approximation in the first

place. Then we have from (21)

$$c_d(k) = \sum_{x\in D_k} c(x,\sigma)\sigma(x) = d_0 \sum_{x\in D_k} \sigma(x)\mathrm{e}^{-\beta(U_0+U(x))}$$

$$= d_0 \sum_{x\in D_k} \sigma(x)\mathrm{e}^{-\beta(U_0+U(x))} = d_0\mathrm{e}^{-\beta(U_0+\bar{U}(k))} \sum_{x\in D_k} \sigma(x) \tag{28}$$

$$= d_0\eta(k)\mathrm{e}^{-\beta(U_0+\bar{U}(k))}$$

since $V(x-y) \equiv J_0$ and

$$U(x) = \bar{U}(k) \qquad \forall\, x \in D_k,$$

which is a direct consequence of the definitions for $U(x)$ and $\bar{U}(k)$, (22) and (7), respectively. In this case the coarse-grained desorption rate above is an exact coarse graining of the original microscopic system, and we obtain the birth–death rates,

$$c_a(k,\eta) = d_0[q-\eta(k)] \qquad \text{and} \qquad c_d(k,\eta) = d_0\eta(k)\mathrm{e}^{-\beta(U_0+\bar{U}(k))}.$$

Although the calculation is exact for any q, we will take $q = N$ since it is the easiest case to implement numerically. In this case we have a single coarse cell and the only order parameter is the total coverage η with rates which simplify even further,

$$c_a^{bd}(\eta) = d_0[q-\eta] \qquad \text{and} \qquad c_d^{bd}(\eta) = d_0\eta\mathrm{e}^{-\beta(U_0+\bar{J}(0,0)(\eta-1)-h(X))}. \tag{29}$$

The resulting process is a Markov birth–death process with a maximum population $q = N$. Based on rates (29) we can now provide the birth–death Markov process generator for η,

$$L_c g(\eta) = c_a(\eta)[g(\eta+1)-g(\eta)] + c_d(\eta)[g(\eta-1)-g(\eta)], \tag{30}$$

where $g \in L^\infty(\mathcal{H}_{1,N}; R)$. Therefore the exact birth–death closure corresponding to the microscopic system (1), (2) is,

$$\text{birth–death closure:} \quad \begin{cases} \dfrac{\mathrm{d}}{\mathrm{d}t}X = \dfrac{1}{\tau_c}(a\eta + b - cX), \\ \dfrac{\mathrm{d}}{\mathrm{d}t}Eg(\eta) = EL_c g(\eta) \qquad \text{where } g \in L^\infty(\mathcal{H}_{1,N}; R). \end{cases} \tag{31}$$

Note further that in the case of $N \to \infty$ (31) easily yields the mean-field closure (15), by employing the corresponding martingale problem, see for instance [5, 8].

We next compare system (31) to (15). The birth–death process η is used as a computational tool in this comparison since it is an exact coarse graining of the microscopic hybrid model.

5.1. Example 1. Oscillatory regime

We choose parameters, shown in the figures, for our hybrid system (1), (2) which create a single unstable node in the corresponding mean-field equation (15) and therefore expect an oscillatory type solution according to the Poincaré–Bendixson theorem (also compare with figure 6.8 in [19]).

We display a typical example for the oscillatory case in figure 5 which quantitatively agrees with the mean-field solution for high q values, whereas the higher noise, lower q system departs from it. Note the random modulation oscillation for $q = 200\,000$. For all simulations undertaken for this oscillatory example, not all of which are shown here, we found that the Curie–Weiss hybrid system (computed exactly via the birth–death process η) did not always produce solutions consistent with the mean-field deterministic closure solutions. This is a somewhat surprising result which shows that although we expect the birth–death closure to produce the same solutions as the mean-field in the limit of $N = q \to \infty$, in reality based on large numerical computations, we obtain disagreements between the two even for very high values of q.

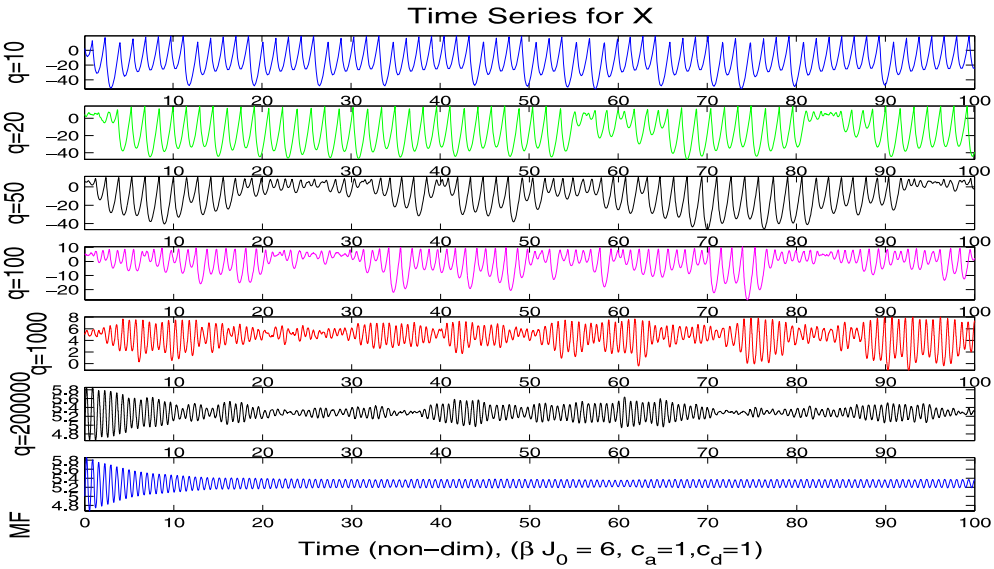

Figure 5. Oscillatory behaviour. Comparisons of birth–death and mean-field solutions for X under the phase transition regime, $\beta J_0 = 6$. Parameters used: $c_a = 1$, $c_d = 1$, $a = 350$, $c = 1$, $b = -200$, $\alpha = 0.1$ and $\gamma = 0$. Initial values $(\bar{\eta}, X) = (0.6, 5)$.

5.2. Example 2. Bistable/metastable regime

For this example we choose parameters for which there are three nodes in the mean-field equation (15): two stable and one unstable. This situation gives rise to more than just multiple solitons or pulses for our hybrid system since now the solutions behave in a metastable manner, visiting the stable nodes between random switching times; see figures 6(*a*)–(*c*). We observe that for low values of q (high noise) random departures occur for the birth–death model from either of the two stable nodes. As expected, the high q case agrees with the deterministic mean-field model.

5.3. Example 3. Excitable/intermittent regime

For the parameter regime provided in figures 7(*a*)–(*c*), the corresponding mean-field system (15) displays only one excitable stable node to which every solution will converge in due time but with large excursions in this adjustment process as in the upper right corner of figure 2. In the hybrid system, this allows solitons and excitable states to occur due to noise and fluctuations even for the case of uniform initial data. Furthermore, it is possible that some of these solutions keep pulsating randomly due to the underlying stochastic noise in our system, thus creating new solitons and an overall strongly intermittent behaviour. Also compare the results above with figure 12.6b on p 328 in [19].

We display only one example in figures 7(*a*)–(*c*) where we observe that multiple pulses are possible for low q values (or high noise levels). The special example of figures 7(*a*)–(*c*) exhibits various types of stochastic oscillation which for the case of $q = 100$ is almost periodic. The periodicity of the random oscillations suggests the existence of a stochastic resonance regime. In fact we have numerically obtained multi-peaked residence time distributions similar to the ones obtained in systems exhibiting stochastic resonance ([4], section IIB). On the other hand note that typically the birth–death solutions for $q = 1000$ display a single pulse and

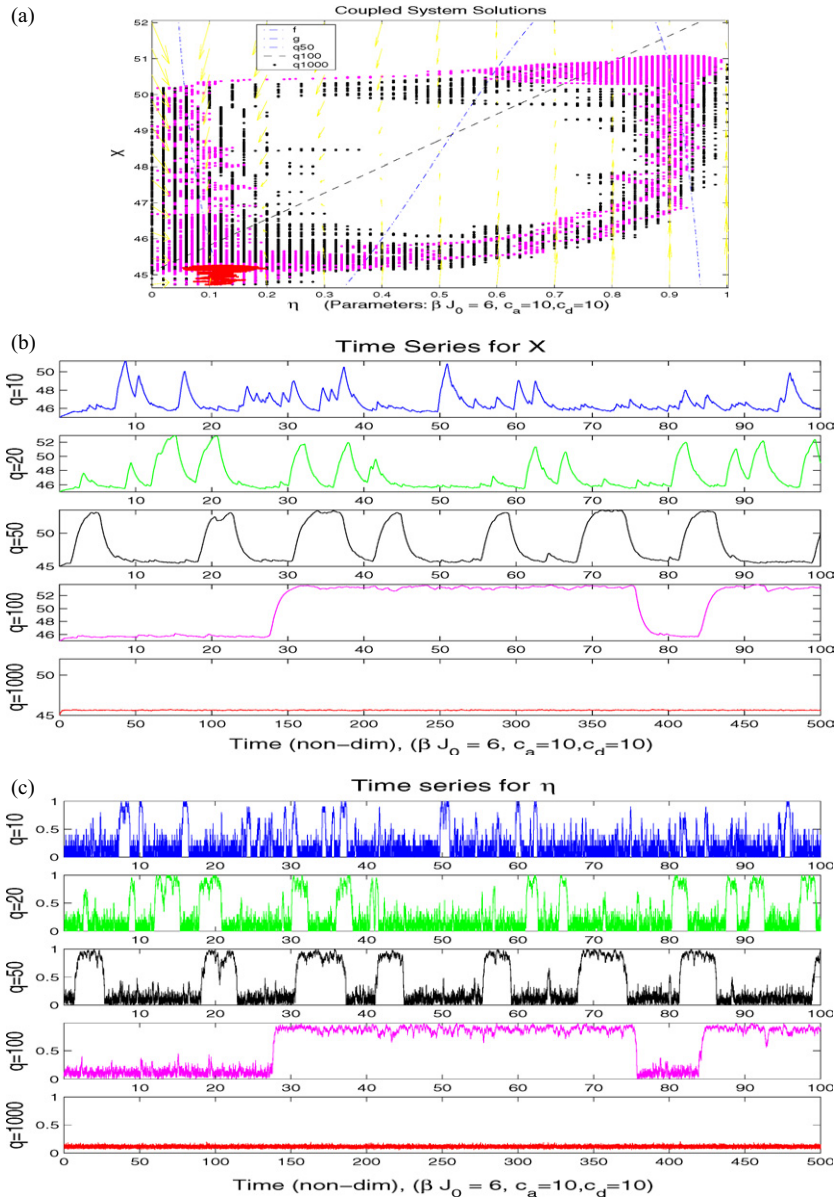

Figure 6. (*a*) Two stable nodes. Birth–death for $q = 50, 100$ and 1000. Coupled system behaviour for the phase transition regime: $\beta J_0 = 6$. Other parameters used: $c_a = c_d = 10$, $a = 10$, $c = 1$, $b = 44.5$, $\alpha = 0.01$ and $\gamma = 0$. Initial values: $(\bar{\eta}, X) = (0.1, 45)$. (*b*) Two stable nodes. Birth–death for $q = 10, 20, 50, 100$ and 1000. Coupled system behaviour for the phase transition regime: $\beta J_0 = 6$. Other parameters used: $c_a = c_d = 10$, $a = 10$, $c = 1$, $b = 44.5$, $\alpha = 0.01$ and $\gamma = 0$. Initial values: $(\bar{\eta}, X) = (0.1, 45)$. (*c*) Two stable nodes. Birth-death for $q = 10, 20, 50, 100$ and 1000. Coupled system behaviour for the phase transition regime: $\beta J_0 = 6$. Other parameters used: $c_a = c_d = 10$, $a = 10$, $c = 1$, $b = 44.5$, $\alpha = 0.01$ and $\gamma = 0$. Initial values: $(\bar{\eta}, X) = (0.1, 45)$.

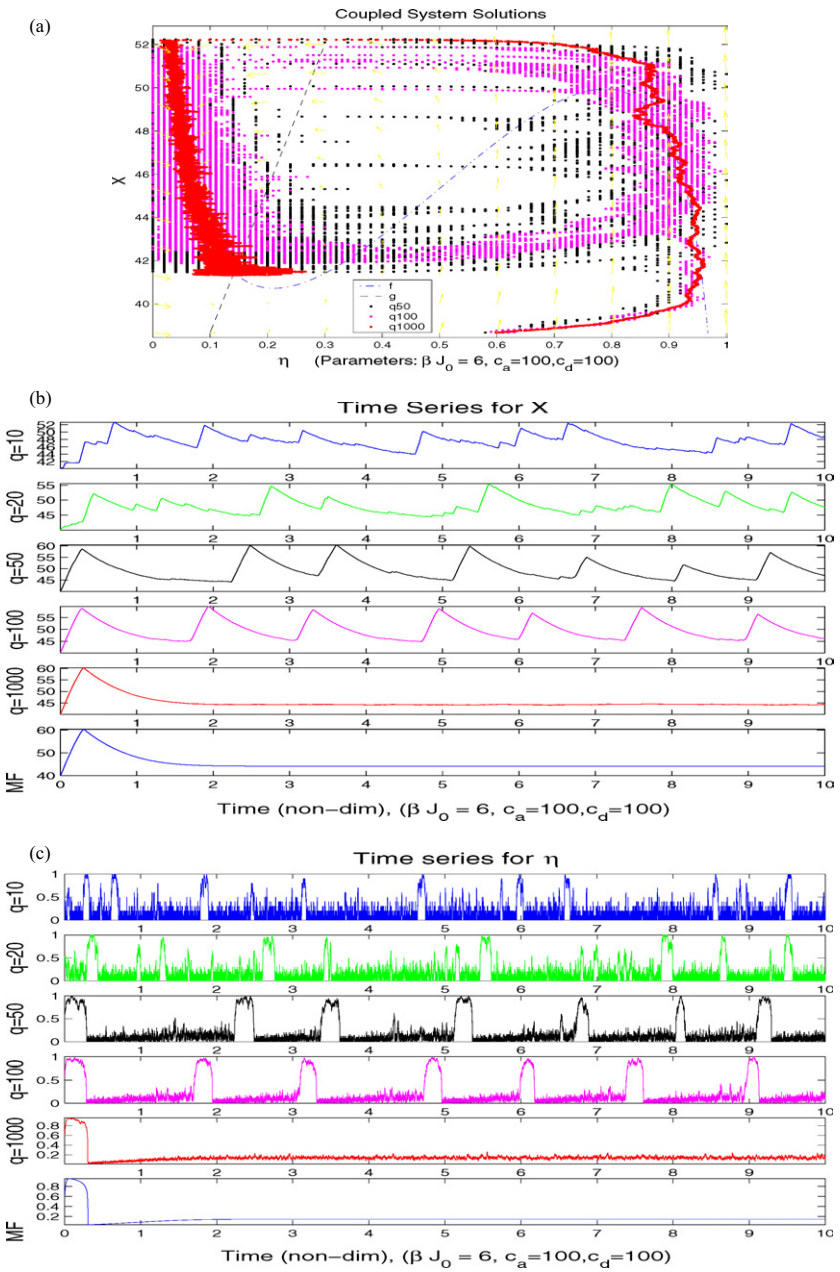

Figure 7. (*a*) Single excitable stable node with multiple pulses. Birth–death for $q = 50$, 100 and 1000. Coupled system behaviour for the phase transition regime: $\beta J_0 = 6$. Other parameters used: $c_a = c_d = 100$, $a = 100$, $c = 1$, $b = 30$, $\alpha = 0.01$ and $\gamma = 0$. Initial values: $(\bar{\eta}, X) = (0.6, 40)$. (*b*) Single excitable stable node with multiple pulses. Birth–death and mean-field solutions for X in the phase transition regime: $\beta J_0 = 6$. Other parameters: $c_a = c_d = 100$, $a = 100$, $c = 1$, $b = 30$, $\alpha = 0.01$ and $\gamma = 0$. Initial values: $(\bar{\eta}, X) = (0.6, 40)$. (*c*) Single excitable stable node with multiple pulses. Birth–death and mean-field solutions for η in the phase transition regime: $\beta J_0 = 6$. Other parameters used: $c_a = c_d = 100$, $a = 100$, $c = 1$, $b = 30$, $\alpha = 0.01$ and $\gamma = 0$. Initial values: $(\bar{\eta}, X) = (0.6, 40)$.

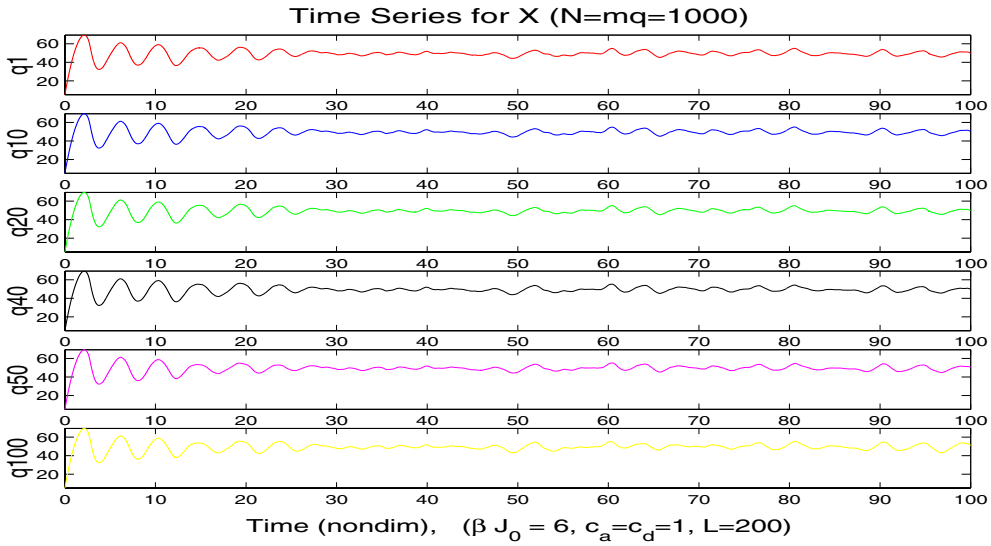

Figure 8. Oscillatory example for $L = 200$. Time series for X for microscopic $q = 1$ and $q = 10, 20, 40, 50, 100$ under the phase transition: $\beta J_0 = 6$. Other parameters: $c_a = c_d = 1$, $a = 100$, $b = 0$, $c = 1$, $\alpha = 0.01$, $\gamma = 0$ and $N = 1000$.

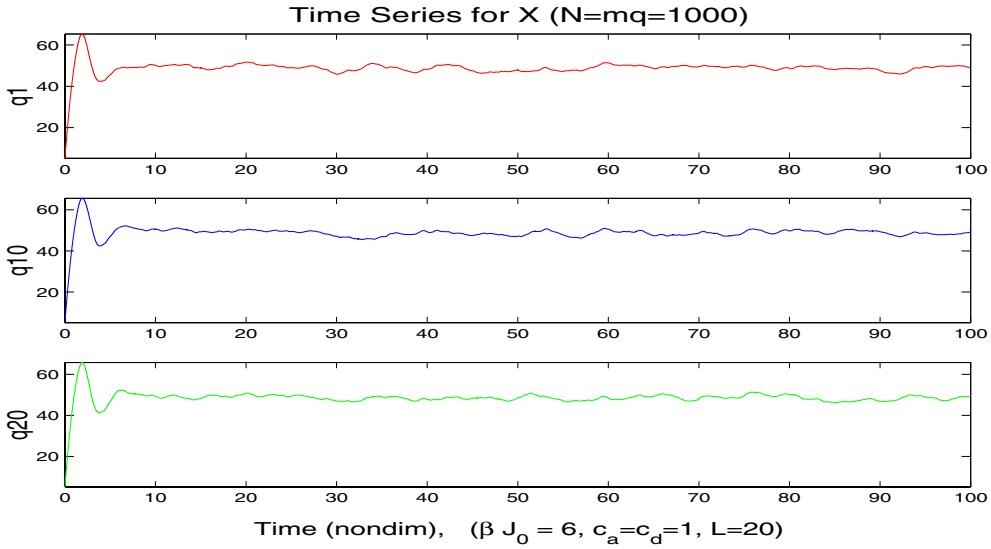

Figure 9. Oscillatory example for $L = 20$. Time series for X for microscopic $q = 1$ and $q = 10$ and 20. This is a phase transition regime since $\beta J_0 = 6$. Other parameters: $c_a = c_d = 1$, $a = 100$, $b = 0$, $c = 1$, $\alpha = 0.01$, $\gamma = 0$ and $N = 1000$.

subsequent approach to the stable node as in the Fitzhugh–Nagumo case [19]. In large time intervals, however, random excitations and rare events will occur [6] which in our simulations here are not observable for the given finite time and because for higher values of q the noise levels are lower.

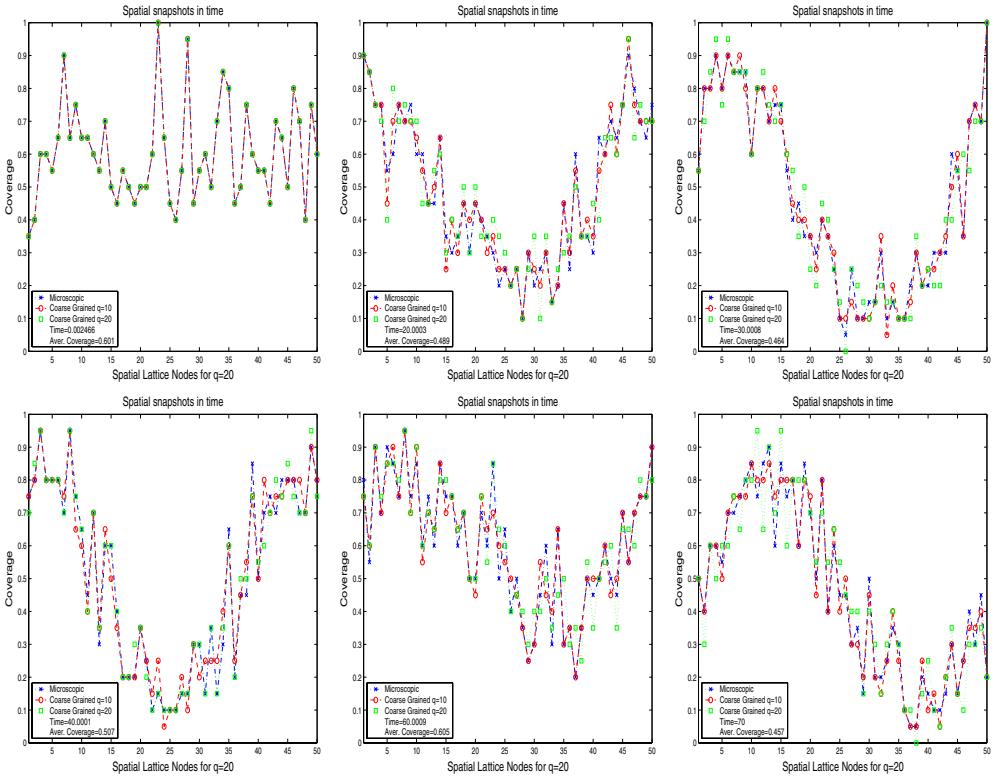

Figure 10. Oscillatory example for $L = 200$. Time series for η between microscopic $q = 1$ and $q = 10, 20$. This a phase transition regime since $\beta J_0 = 6$. Other parameters: $c_a = c_d = 1$, $a = 100$, $b = 0$, $c = 1$, $\alpha = 0.01$, $\gamma = 0$ and $N = 1000$.

There are two main attributes in our stochastic lattice model which we must keep track of: the size of the system and noise. In fact the size of the system and noise levels are directly related to each other since large lattices display low noise levels and vice versa. In general we observe that solutions and comparisons between the mean-field and birth–death closures depend heavily on the size of the system. Fluctuations are similarly important even if N is big as can be seen in these examples. This is evident in all cases where for high noise (small lattice sizes) the birth–death model shows a completely different stability behaviour compared to what it does for low noise systems. Furthermore we observed disagreement between the two closures even for very large system sizes (see figure 5) where theoretically—at least as $N \to \infty$—they should agree. Another issue arises also in the case where the birth–death closure correctly predicts one of the two stable nodes, in figure 6(c) for $q = 1000$, in the bistable example. The birth–death process, given long enough time, should visit the other node giving rise to a metastable behaviour. Therefore, based on this discussion and the examples presented, the mean-field closure cannot capture the complete transient and long time dynamics of (31).

6. Coarse-grained simulations and statistical analysis

In this section we examine the coarse-grained closure approximation presented in section 4 for the coupled spin flip dynamics in the general case where we have microscopic interactions of size L in (22). We present numerical simulations and comparisons against the microscopic

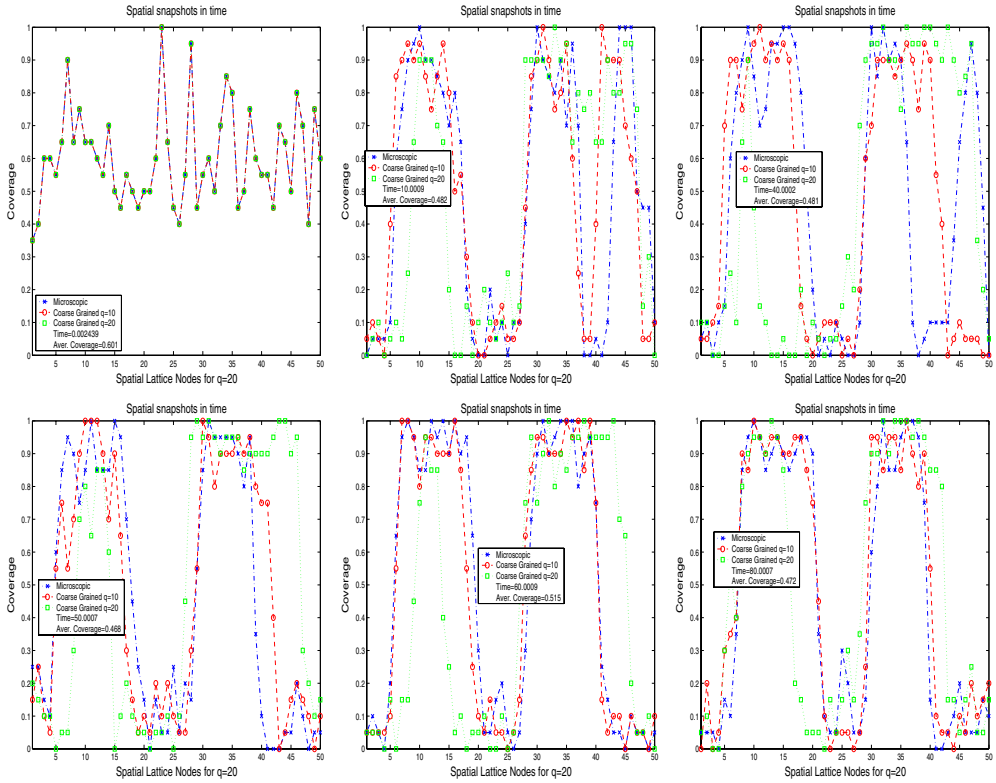

Figure 11. Oscillatory example for $L = 20$. Snapshots in time for η between microscopic $q = 1$ and $q = 10, 20$. This a phase transition regime since $\beta J_0 = 6$. Other parameters: $c_a = c_d = 1$, $a = 100$, $b = 0$, $c = 1$, $\alpha = 0.01$, $\gamma = 0$ and $N = 1000$.

hybrid system and in the process we test the influence of parameters and extent to which we may apply this coarse-graining method in the phase transition regime. In some cases we carry out pathwise comparisons of the solutions. However, in the intermittent example pulses occur instantaneously, are short lived, and are harder to compare against the microscopic solution in a pathwise manner. Similar challenges arise in the oscillatory case. We therefore provide a detailed statistical signal analysis which consists of auto-correlations, periodograms and cross-correlations and is carried out on very long signals although in the figures we only display a representative small part. We compare various coarse grainings against the hybrid system (1), (2) under different parameter regimes in order to assess the validity of the coarse graining approach; we further probe numerically the extent to which the assumption $q \ll L$ (or even $q = L$) remains valid and capable of maintaining a reasonably accurate approximation.

6.1. Example 1. Oscillatory regime

In this subsection we examine our hybrid system (1), (2) under the phase transition regime $\beta J_0 = 6$ for the case where the mean-field ODE (15) displays oscillatory behaviour. We apply parameters similar to those chosen for the equivalent oscillatory example in section 5. In figures 8–11 which follow in this subsection we examine both long ($L = 200$) and short ($L = 20$) range potentials and their effect in the hybrid coupling. We also compare

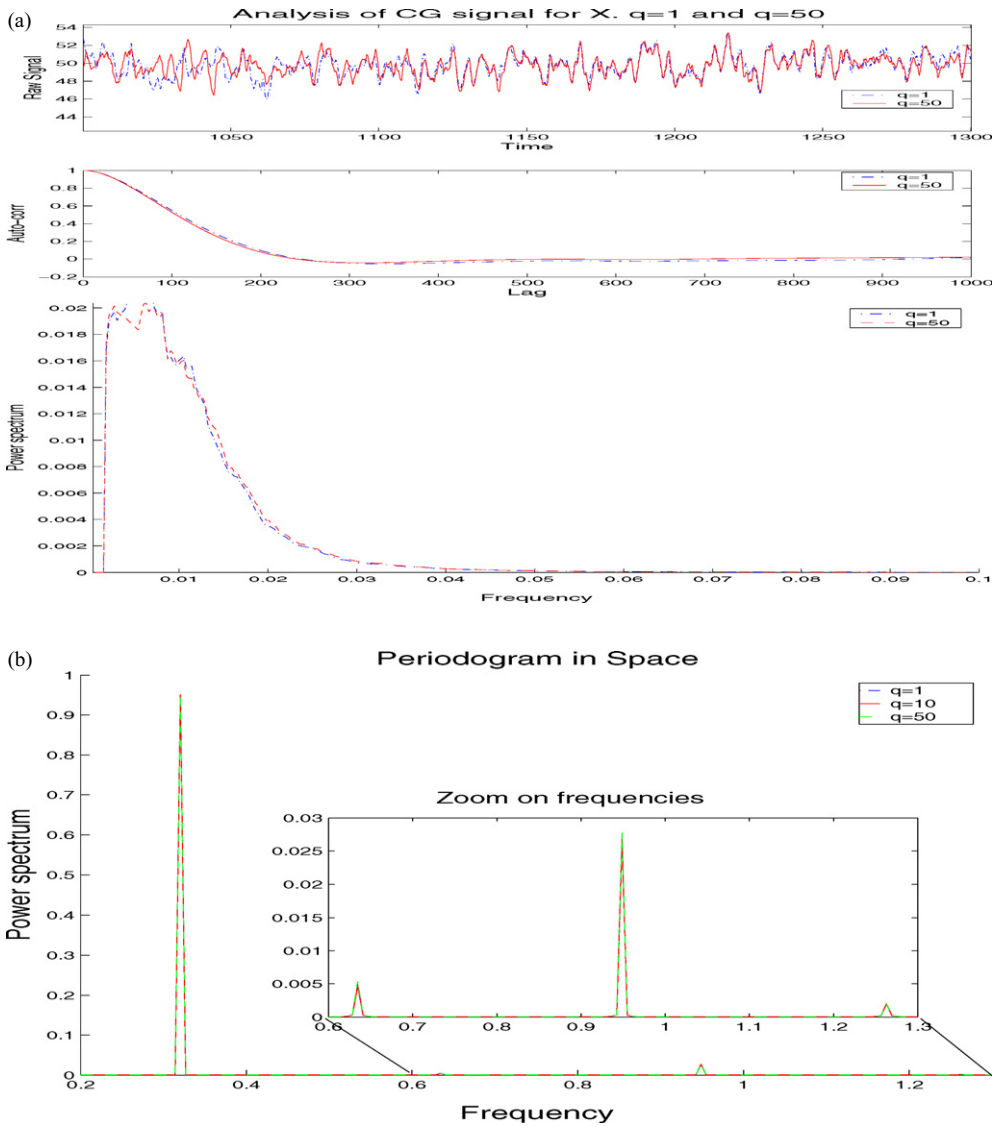

Figure 12. (*a*) Comparisons for oscillatory case on signal from X with $L = 100$. Timeseries, auto-correlation and spectrum analysis for the cases of $q = 1$ and $q = 50$ with $\beta J_0 = 6$. (*b*) Spatial comparisons for X in the oscillatory case with $L = 100$. Spatial spectrum analysis for the cases of $q = 1, 10$ and 50. For this comparison spatial domains are adjusted to that corresponding to $q = 50$ (i.e. $m = 20$, where $N = mq$) with $\beta J_0 = 6$. (*c*) Oscillatory case. Cross-correlations in time between X and η for $q = 1, 10$ and 50 while $\beta J_0 = 6$ and $L = 100$.

snapshots in time of the spatial distribution of the stochastic model after each example is presented.

Overall we observe a marked difference between the two simulations which is attributed to the size of L. As expected, based on our theorem 4.1, the effect of the size of the potential range is important. Although the agreement is quite good in both time and space between these solutions, our comparisons show that the error in the case of $L = 20$ is higher, as can be

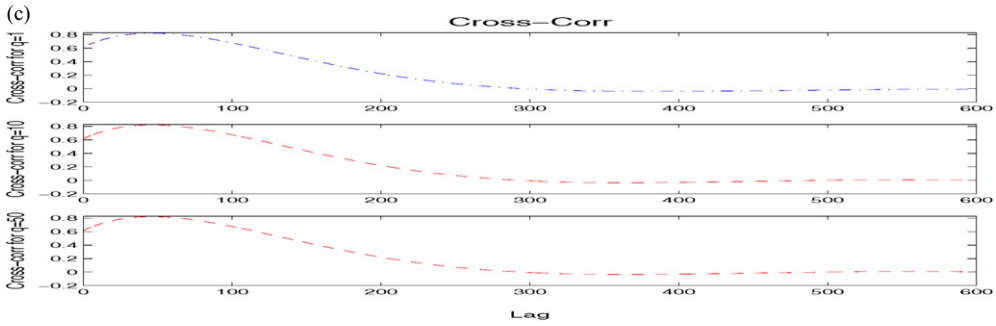

Figure 12. (Continued).

seen in figure 11, when compared against the microscopic solution since q is very close to the size of L.

Furthermore we note that in several examples, not all presented here, the spatial distribution of the stochastic model takes the form of a sinusoidal wave. This can also be seen in figures 10 and 11. In both these spatial distributions we note that we do obtain the correct averaged behaviour for the coupled system in time although the underlying spatial behaviour is quite different! Specifically we obtain the correct average coverage, which is around 0.5, for both examples as can be seen in figures 10 and 11. However, figure 10 displays a sinusoidal wave while figure 11 has of two islands which maintain their profile essentially unaltered through time. In that respect we undertake further simulations in figures 12(*a*)–(*c*) over very long signals and perform a statistical signal analysis in time and space in order to compare the main features of our microscopic and coarse-grained signals. The signal analysis undertaken reveals the following:

- Case of $q = 1$ versus $q = 10$: we verify once again that we have excellent agreement between coarse-grained and microscopic dynamics. See also the cross-correlations in figure 12(*c*).
- Case of $q = 1$ versus $q = 50$: similarly good agreement is seen for this case when compared with the microscopic dynamics in figures 12(*a*) and (*b*), although a bit unexpected, based on theorem 4.1, since $q = 50$ is considered to be high compared to the potential radius of $L = 100$.

Finally, the spatial ensemble periodogram presented in figure 12(*b*) displays remarkable agreement in spatial frequency space. The cross-correlations between the solutions X and η for each dynamics considered are also presented in figure 12(*c*) and seem to be highly correlated under all dynamics, $q = 1$, 10 and 50, presented.

6.2. Example 2. Excitable/intermittent regime

We now examine the excitable case for our hybrid system (1), (2) under the phase transition regime $\beta J_0 = 6$ with the same parameters as those chosen for the examples in section 5. The parameters are chosen in such a way that the hybrid system remains in the excitable/intermittent regime producing a pulsating phenomenon. As usual in order to draw our conclusions we compare the time series as well as spatial snapshots in time of the distribution of the stochastic model.

We display the time series behaviour in figures 13(*a*), (*b*) and 14(*a*), (*b*). The parameters as usual are provided in the figures (see also figure 15). Note that in this example we have the

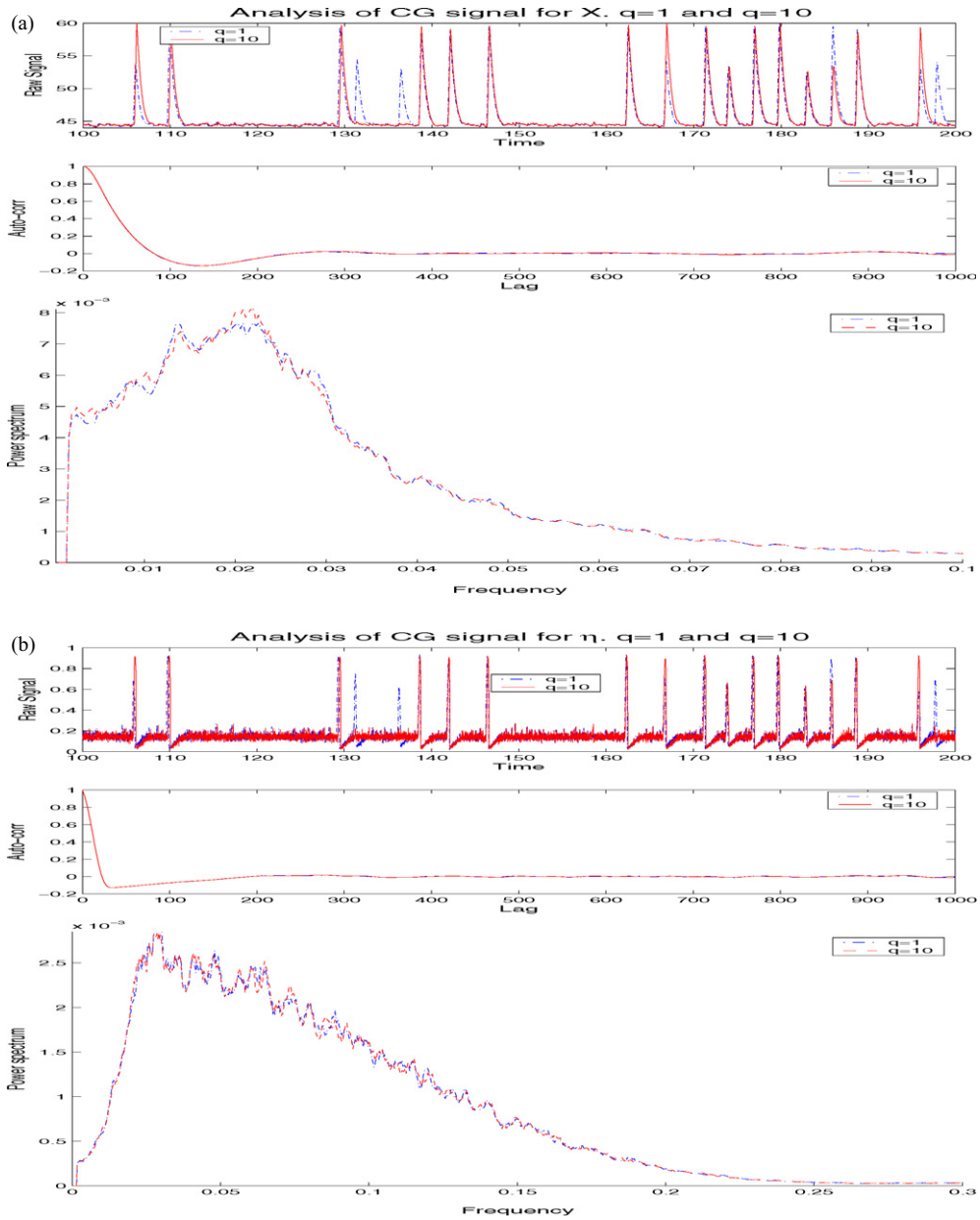

Figure 13. (*a*) Comparisons for X in the excitable case. Time series, auto-correlation and spectrum analysis for the cases of $q = 1$ and 10. Parameters: $L = 100$, $N = 1000$ and $\beta J_0 = 6$. (*b*) Comparisons for excitable case on signal from η. Time series, auto-correlation and spectrum analysis for the cases of $q = 1$ and 10. Parameters: $L = 100$, $N = 1000$ and $\beta J_0 = 6$.

phenomenon of strong intermittency. We observe disagreement in these simulations in both spatial and temporal variables of interest between $q = 1$ and any of the other coarse graining examined. However, statistical signal analysis may allow us to see sometimes hidden trends over long times. Overall we observe good agreement for the case of $q = 10$ and $q = 1$ in

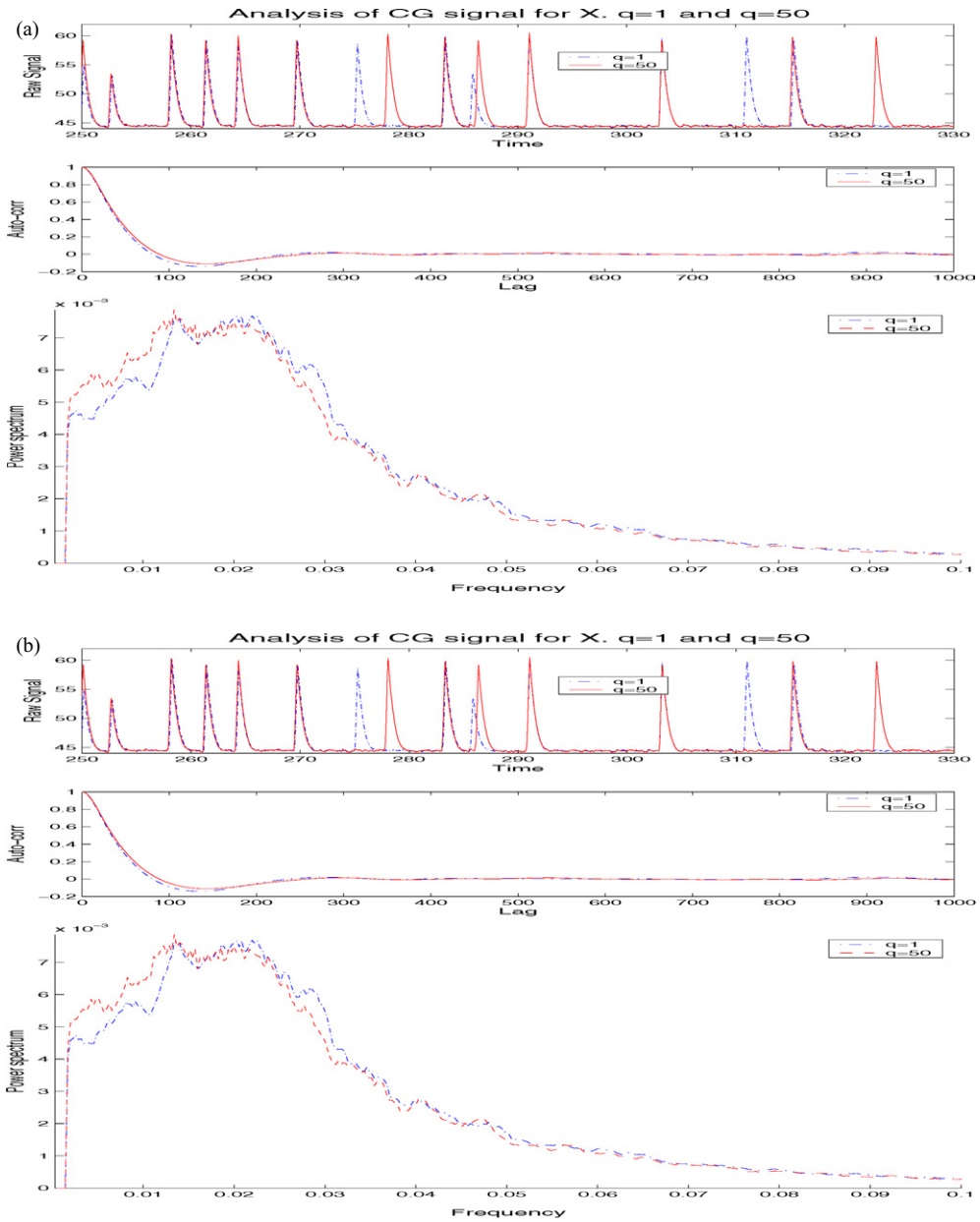

Figure 14. (*a*) Comparisons for excitable case on signal from X. Time series, auto-correlation and spectrum analysis for the cases of $q = 1$ and 50. Parameters: $L = 100$, $N = 1000$ and $\beta J_0 = 6$. (*b*) Comparisons for excitable case on signal from η. Timeseries, auto-correlation and spectrum analysis for the cases of $q = 1$ and 50. Parameters: $L = 100$, $N = 1000$ and $\beta J_0 = 6$. (*c*) Spatial comparisons for X in the excitable case. Spatial spectrum analysis for the cases of $q = 1$, 10 and 50. For this comparison spatial domains are adjusted to that corresponding to $q = 50$ (i.e. $m = 20$, where $N = mq$). Parameters: $L = 100$, $N = 1000$ and $\beta J_0 = 6$.

(c)

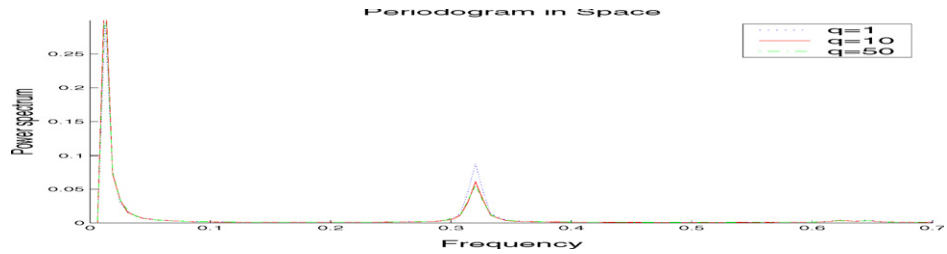

Figure 14. (Continued).

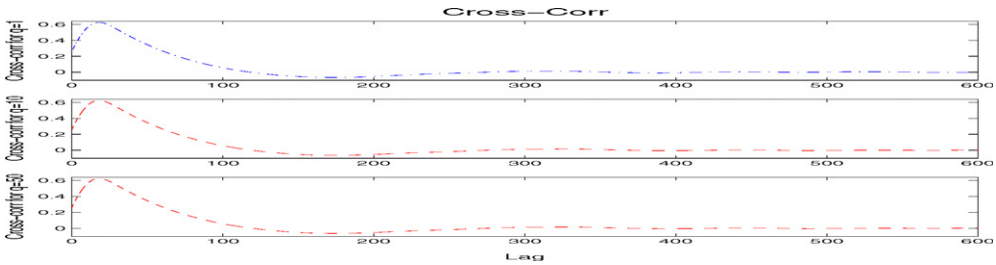

Figure 15. Excitable case. Cross-correlations in time between X and η for $q = 1, 10$ and 50. Parameters: $L = 100$, $N = 1000$ and $\beta J_0 = 6$.

Table 2. Excitable case. CPU times for solutions of the microscopic hybrid system and the corresponding coarse-grained closure. Parameters: $L = 100$, $N = 1000$.

q	1	10	20	50
CPU time (s)	2 412 131	27 122	9 150	2281

Table 3. Oscillatory case. CPU times for solutions of the microscopic hybrid system against the corresponding coarse-grained closure. Parameters: $N = 1000$.

q	1	10	20	40	50	100
For $L = 200$						
CPU time (s)	19 520	407	108	33	22	7
q	1	10	20			
For $L = 20$						
CPU time (s)	213	55	18			

figures 13(*a*) and (*b*) as can be seen by the periodograms included therein. This is expected since according to theorem 4.1 q is small enough compared to L and the approximation does not produce much error. Remarkably the cases of $q = 1$ and $q = 50$ as presented in the ensemble periodograms in figures 14(*a*) and (*b*) also display good agreement although you might have thought otherwise by simply comparing the raw signal included in these figures.

Overall we note that the coarse-grained strategy has been systematically tested in the most demanding regimes and performs extremely well in terms of error of approximation. We further provide l_1 error estimates in table 2 for the differences observed in the ensemble

Table 4. The l_1 error estimate between microscopic and coarse-grained solutions for the oscillatory ($L = 200$) and excitable ($L = 100$) examples in this section.

Type	$\|X_{q1} - X_{q10}\|_1$	$\|u_{q1} - u_{q10}\|_1$	$\|X_{q1} - X_{q50}\|_1$	$\|u_{q1} - u_{q50}\|_1$
Osc.	0.3×10^{-5}	0.3×10^{-5}	0.5×10^{-5}	0.5×10^{-5}
Exc.	0.3×10^{-5}	0.3×10^{-5}	0.7×10^{-5}	0.5×10^{-5}

power spectrum for both the examples above (we only present the case with $L = 200$ for the oscillatory case). Similarly the CPU savings, which were reported earlier in section 4.1 and here in tables 2 and 3 for each example, are substantial (see also table 4).

7. Conclusions and discussion

Hybrid systems arising in numerous applied fields exhibit a host of complex behaviours that pose challenges both in their direct numerical implementation and simulation, and in the interpretation of their behaviour through suitable analysis. These questions were one of the principal motivations behind introducing the model hybrid systems in [5, 6], as well as in the present paper. Such systems capture the essential features of their complex hybrid counterparts but allow the developing and testing of computationally inexpensive mesoscopic deterministic and stochastic closures in various asymptotic limits. Furthermore, they allow computationally feasible detailed statistical comparisons of the derived mesoscopic theories (mean-field, local mean-field and stochastic averaging approximations) against direct numerical simulations of the full hybrid system.

In conclusion, we summarize the proposed approach for hybrid systems with complex behaviour as follows. (a) Mean field and other deterministic closure approximations can provide an initial insight into the dynamic behaviour of the entire hybrid system. In our case in the presence of strong interactions the mean-field model is a Fitzhugh–Nagumo type system. (b) When the mean-field system has nontrivial behaviour (multiple steady states, oscillations, excitable regimes, bifurcations, etc) it is reasonable to assume that stochastic fluctuations can play a dominant role in the transient and long-time behaviour, altering the mean-field picture. (c) Computationally efficient stochastic closures of the hybrid system were derived based on hierarchical coarse grainings of the lattice model; these coarse-grained hybrid systems showed statistical agreement with the full system even in regimes dominated by the interaction of nonlinearity and random fluctuations, such as regimes of strong intermittency, metastability and random oscillations.

Acknowledgments

The research of MAK is partially supported by NSF-DMS-0413864, NSF-ITR-0219211 and DE-FG02-05ER25702 and the research of AJM is partially supported by ONR N00014-05-1-0164 and NSF-DMS-0456713.

References

[1] Ellis R 1985 *Entropy, Large Deviations, and Statistical Mechanics* (Berlin: Springer)
[2] E W and Engquist B 2003 The heterogeneous multiscale method *Commun. Math. Sci.* **1** 87–133
[3] Friedlin M I and Wentzell A D 1998 *Random Perturbations of Dynamical Systems* (Berlin: Springer)
[4] Grammaitoni L, Hanggi P, Jung P and Mardesoni F 1998 Stochastic resonance *Rev. Mod. Phys.* **70** 223–87

[5] Katsoulakis M A, Majda A J and Sopasakis A 2004 Multiscale couplings in prototype hybrid deterministic/stochastic systems: part I, deterministic closures *Commun. Math. Sci.* **2** 255–94
[6] Katsoulakis M A, Majda A J and Sopasakis A 2005 Multiscale couplings in prototype hybrid deterministic/stochastic systems: part II, stochastic closures *Commun. Math. Sci.* **3** 453–78
[7] Katsoulakis M A, Majda A J and Vlachos D G 2003 Coarse-grained stochastic processes and Monte Carlo simulations in lattice systems *J. Comput. Phys.* **186** 250–78
[8] Katsoulakis M A, Majda A J and Vlachos D G 2003 Coarse-grained stochastic processes for lattice systems *Proc. Natl Acad. Sci. USA* **100** 782–7
[9] Katsoulakis M A, Plecháč P and Sopasakis A 2005 Error control and analysis in coarse-graining of stochastic lattice dynamics *Preprint* math/0509228
[10] Katsoulakis M A and Trashorras J 2006 Information loss in coarse-graining of stochastic particle dynamics *J. Stat. Phys.* **122** 115–35
[11] Katsoulakis M A and Vlachos D G 2003 Coarse-grained stochastic processes and kinetic Monte Carlo simulations for the diffusion of interacting particles *J. Chem. Phys.* **119** 9412
[12] Kevrekidis I G, Gear C W, Hyman J, Kevrekidis P G, Runborg O and Theodoropoulos C 2003 Equation-free, coarse-grained multiscale computation: enabling microscopic simulators to perform system-level tasks *Commun. Math. Sci.* **1** 715–62
[13] Kevrekidis I G, Schmidt L D and Aris R 1984 *Surf. Sci.* **137** 151
[14] Khouider B, Majda A J and Katsoulakis M A 2003 Coarse-grained stochastic models for tropical convection and climate *Proc. Natl Acad. Sci. USA* **100** 11941–6
[15] Kipnis C and Landim C 1999 *Scaling Limits of Interacting Particle Systems* (Berlin: Springer)
[16] Lam R and Vlachos D G 2001 Multiscale model for epitaxial growth of films: growth mode transition *Phys. Rev.* B **64** 35401
[17] Lavis D A and Bell G M 1999 *Statistical Mechanics of Lattice Systems 1: Closed-Form and Exact Solutions* (Berlin: Springer)
[18] Majda A J and Khouider B 2002 Stochastic and mesoscopic models for tropical convection *Proc. Natl Acad. Sci. USA* **99** 1123
[19] Murray J D 1989 *Mathematical Biology* (Berlin: Springer)
[20] Oettinger H C and Laso M 2004 CONNFFESSIT: Simulating polymer flow *Simulation Methods for Polymers* chapter 16 ed M J Kotelyanski and D N Theodorou (Boca Raton, FL: CRC Press) pp 511–58
[21] Rodgers S T and Jensen K F 1998 Multiscale modeling of chemical vapor deposition. *J. Appl. Phys.* **83** 524
[22] Thomas T M and Cover J A 1991 *Elements of Information Theory* (New York: Wiley)
[23] Vlachos D G, Schmidt L D and Aris R 1990 The effects of phase transitions, surface diffusion and defects on surface catalyzed reactions: fluctuations and oscillations *J. Chem. Phys.* **93** 8306
[24] Wiley H S, Shvartsman S Y and Lauffenburger D A 2003 Computational modeling of the EGF receptor system: a paradigm for systems biology. *Trends Cell Biol.* **13** 43–50